Available online at www.sciencedirect.com
SCIENCE DIRECT®
Powder Technology 166 (2006) 1 – 13
POWDER TECHNOLOGY
www.elsevier.com/locate/powtec

Sedimentation of a cylindrical particle along the axis of a cylindrical tube filled with Carreau fluid

Jyh-Ping Hsu [a,*], Wei-Jyh Chen [a], Shiojenn Tseng [b], Chur-Jen Chen [c]

[a] *Department of Chemical Engineering, National Taiwan University, Taipei, Taiwan 10617*
[b] *Department of Mathematics, Tamkang University, Tamsui, Taipei, Taiwan 25137*
[c] *Department of Mathematics, Tunghai University, Taichung, Taiwan 403*

Received 14 September 2005; received in revised form 20 January 2006; accepted 18 May 2006

Abstract

The boundary effect on the movement of a particle in a Carreau fluid is investigated theoretically by considering the sedimentation of a cylindrical particle along the axis of a cylindrical tube. The influences of the key parameters of the system under consideration on the drag coefficient and the associated flow field are discussed. These include the relaxation time constant and the power-law index of a Carreau fluid, the length of a particle, and the diameter of a cylindrical tube. We show that the flow field and the drag coefficient are affected more significantly by the boundary effect, measured by the ratio (particle diameter/tube diameter) than by the size of a particle and the properties of the fluid. In general, the terminal velocity of a particle correlates nonlinearly with the ratio (particle diameter/tube diameter). The problem of a particle in an unbounded fluid can be recovered as a limiting case of the present one.

Keywords: Sedimentation; Boundary effect; Cylinder in cylindrical tube; Carreau fluid; Drag coefficient

1. Introduction

Although available results for the sedimentation of a particle in a boundary-free medium are ample in the literature, those for the case when a boundary is present, which is ubiquitous in practice, are relatively limited. The presence of a boundary has the effect of retarding the sedimentation of a particle, in general. The flow field surrounding the latter is inevitably influenced by the former, and, as a result, the sedimentation velocity of the latter is reduced. For a non-Newtonian fluid, since its viscosity might be position dependent, the boundary effect on the sedimentation of a particle can be profound. A wall factor, defined as the ratio (terminal velocity when boundary is present/terminal velocity when boundary is absent), is usually used to measure the boundary effect on the sedimentation behavior of a particle. This factor is a function of Reynolds number, and the geometry and orientation of a particle. Tripathi et al. [1] investigated theoretically the drag coefficients of a sphere and a spheroid in a shear-thinning power-law fluid. Tripathi and Chhabra [2] discussed the relation between the drag coefficient of a spheroid in a shear-thickening, power-law fluid and Reynolds number. Under the condition of low Reynolds number, Missirlis et al. [3] studied the wall effects for the motion of a sphere in a shear-thinning power-law fluid. Chhabra [4,5] observed the sedimentation of particles of various shapes in a cylindrical tube filled with a shear-thinning, power-law fluid and obtained a linear relation between the wall factor and Λ=(diameter of equivalent sphere/diameter of boundary) for disk, cylinder, and rectangular prism under the conditions that Reynolds number is smaller than 7 and $\Lambda<0.5$. The results obtained are consistent with experimental observations, and are applicable to Reynolds number up to about 1000 and the index parameter ranges from 0.5 to 1. Machač et al. [6,7] performed the sedimentation of both spherical and non-spherical particles in a Carreau fluid at low Reynolds number; numerical simulation was also conducted based on Hill's variational principles. Chhabra and Uhlherr [8] conducted the sedimentation of a sphere in a Carreau fluid at a high Reynolds number. They obtained an empirical expression which correlates drag coefficient with Reynolds number and the key parameters of a fluid. The boundary effect on the

* Corresponding author. Tel.: +886 2 23637448; fax: +886 2 23623040.
E-mail address: jphsu@ntu.edu.tw (J.-P. Hsu).

0032-5910/$ - see front matter © 2006 Elsevier B.V. All rights reserved.
doi:10.1016/j.powtec.2006.05.003

sedimentation of a sphere in a Bingham fluid was studied theoretically by Blackery and Mitsoulis [9] at low Reynolds numbers. Unnikrishnan [10] and Chhabra [11] examined the boundary effect on the sedimentation of both a sphere and a cylinder in both Newtonian and non-Newtonian fluids. Hsu et al. [12] modeled theoretically the sedimentation of a spheroid in a cylindrical tube filled with a Carreau fluid.

For a non-Newtonian fluid, the viscosity–shear rate relation is its most important property to the sedimentation problem under consideration since the drag on a particle is directly related to that relation. Among proposed relations for non-Newtonian systems, the Carreau model is found to be appropriate for general purposes [13]. The constitutive equations for a Carreau fluid are [13]

$$\boldsymbol{\tau} = -\eta(\dot{\boldsymbol{\gamma}})\dot{\boldsymbol{\gamma}} = -[\eta_\infty + (\eta_0 - \eta_\infty)[1 + (\lambda\dot{\boldsymbol{\gamma}})^\beta]^{(n-1)/\beta}]\dot{\boldsymbol{\gamma}} \quad (1)$$

$$\dot{\boldsymbol{\gamma}} = \nabla v + (\nabla v)^T \quad (2)$$

In these expressions, $\boldsymbol{\tau}$ and $\dot{\boldsymbol{\gamma}}$ are respectively the stress tensor and the rate of strain tensor, v is the velocity, and ∇ and T are respectively the gradient operator and matrix transpose. η is the apparent viscosity, and η_0 and η_∞ are respectively the zero-shear-rate viscosity and infinite-shear-rate viscosity. λ, n, and β are respectively the relaxation time constant, the power-law exponent, and a dimensionless parameter describing the transition region between the zero-shear-rate region and the power-law region. Note that if $n \to 1$ and/or $\lambda \to 0$, Eq. (1) describes a Newtonian fluid; if λ is sufficiently large, it describes a power-law fluid.

Recently, Hsu et al. [14] evaluated the drag on an isolated cylindrical particle in an infinite Carreau fluid, that is, the boundary effect on sedimentation is neglected. Their analysis is extended in this study to the case when a boundary effect can be significant by considering the sedimentation of a cylindrical particle along the axis of a cylindrical tube filled with a Carreau fluid. Numerical simulations are conducted to examine the influences of the key parameters of the system under consideration, including the relaxation time constant and the power-law index of a Carreau fluid, the length of a particle, and the diameter of a cylindrical tube, on the drag coefficient and the associated flow field.

2. Theory

Let us consider the sedimentation of a cylindrical particle of length L and diameter d_c with a constant velocity along the axis of a cylindrical tube of diameter D which is filled with an incompressible Carreau fluid. As shown in Fig. 1, we assume for convenience that the particle is held fixed and the liquid flows with bulk velocity $\mathbf{u_t}$ and speed u_t. The cylindrical coordinates (r,θ,z) with its origin located at the axis of the tube are adopted. In practice, β can be assumed the value of 2 and η_∞ is negligible. Therefore Eq. (1) reduces to

$$\eta(\dot{\gamma}) = \eta_0[1 + (\lambda\dot{\gamma})^2]^{(n-1)/2} \quad (3)$$

where $\dot{\gamma}$ and is the shear rate. Note that the smaller the value of n and/or the larger the value of λ, the more non-Newtonian a fluid is.

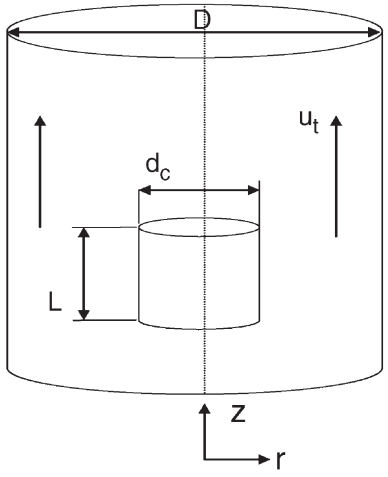

Fig. 1. Schematic representation of the problem considered where a rigid cylindrical particle of length L and diameter d_c in a cylindrical tube filled with a Carreau fluid. For convenience, the particle is held fixed in the liquid phase and the bilk fluid flows with the relative velocity $\mathbf{u_t}$. The cylindrical coordinates (r,θ, z) with its origin located at the axis of the tube are adopted.

For illustration, we assume that η_0=6.7 g cm/s [5]. The flow field at steady state can be described by

$$\nabla \bullet \mathbf{u} = 0 \quad (4)$$

$$\rho\mathbf{u} \bullet \nabla\mathbf{u} = -\nabla P + \nabla \bullet (\eta\nabla\mathbf{u}) \quad (5)$$

where $\bullet\ \bullet$ is the gradient operator, $\mathbf{u}$ and ρ are respectively the velocity and the density of the fluid, and P is the pressure. Since the particle is fixed and the bulk fluid velocity and speed are $\mathbf{u_t}$ and u_t respectively, we have the following boundary conditions:

$$u_Z = u_t, r = D/2 \quad (6)$$

$$u_Z = u_t \text{ as } z \to \infty \quad (7)$$

$$\mathbf{u} = 0 \text{ on particle surface} \quad (8)$$

$$\frac{\partial \mathbf{u}}{\partial r} = 0,\ r = 0 \quad (9)$$

$$u_\theta = 0 \quad (10)$$

For a cylindrical particle in a Carreau fluid the drag coefficient C_D can be expressed as [7]

$$C_D = \frac{24}{Re}\left(\frac{d_v}{d_n}\right)^2 \frac{Z(Cu,n)}{\varphi_N} \quad (11)$$

where $Re = \rho u_t d_v/\mu$ is the Reynolds number, d_v is the diameter of a sphere which has the same volume as the particle, d_n is the diameter of the circle which has the same area as that of the projection of the particle on a plane perpendicular to the movement of the particle, Z is a correction function, and φ_N is a dynamic shape correction factor, which depends on the

Table 1
Comparison between the drag force evaluated by the present method when $D\to\infty$,F_D^∞, with the corresponding result of Machač et al. [7], F_D', at various n, (a), and at various λ, (b), for the case when $L/d_c=0.1$

(a)			
$\lambda=0.1887$ s	$n=0.2$	$n=0.5$	$n=0.8$
u_∞ (cm/s)	14.1740	5.1961	3.7071
F_D^∞ (g cm/s^2)	55.4193	55.4193	55.4193
F_D' (g cm/s^2)	84.5555	49.1797	47.9343
(b)			
$n=0.5$	$\lambda=0.1887$ s	$\lambda=5.1887$ s	$\lambda=9.1887$ s
u_∞ (cm/s)	0.9528	6.3045	9.5371
F_D^∞ (g cm/s^2)	14.6874	14.6874	14.6874
F_D' (g cm/s^2)	11.5756	11.5237	11.2608

Table 3
Comparison between the drag force evaluated by the present method when $D\to\infty$, F_D^∞, with the corresponding result of Machač et al. [7], F_D', at various n, (a), and at various λ, (b), for the case when $L/d_c=3.33$

(a)			
$\lambda=0.1887$ s	$n=0.2$	$n=0.5$	$n=0.8$
u_∞ (cm/s)	7.4682	3.8717	3.1739
F_D^∞ (g cm/s^2)	100.0503	100.0503	100.0503
F_D' (g cm/s^2)	141.8088	92.5100	90.3343
(b)			
$n=0.5$	$\lambda=0.1887$ s	$\lambda=5.1887$ s	$\lambda=9.1887$ s
u_∞ (cm/s)	1.0623	6.2968	9.8386
F_D^∞ (g cm/s^2)	34.0000	34.0000	34.0000
F_D' (g cm/s^2)	29.4138	39.1965	39.0072

orientation of the sedimentation. For the present case, Z can be expressed as [7]

$$Z(Cu,n)=\{1+[(Z_1+Z_2n+Z_3n^2)\Lambda]^{Z_4}\}^{n-1/2} \tag{12}$$

where $Cu=2\lambda u/d_v$ and $\Lambda=d_v/D$. This expression is applicable for $0.3<n<1.0$. If $0<Cu\leqq 50$, then $Z_1=0.707$, Z_20, $Z_3=2.433$, and $Z_4=0.736$; if $50<Cu\leqq 410$, then $Z_1=0.780$, $Z_2=-1.857$, $Z_3=1.944$, and $Z_4=1.744$. The correction factor φ_N can be expressed as [7]

$$\log\varphi_N=\left[\frac{-0.270}{\sqrt{\psi}(d_v/d_n)^{0.345}}\left(\frac{d_v}{d_n}-1\right)+\log\left(\frac{d_v}{d_n}\sqrt{\psi}\right)\right] \tag{13}$$

where ψ is the ratio (surface area of cylinder/surface area of equivalent sphere). For the present case, u_t can be expressed as [7]

$$u_t=\frac{gd_v^2(\rho_s-\rho)}{18\eta_0}\frac{\varphi_N}{Z(\mathrm{Cu,n})} \tag{14}$$

where g is the gravitational acceleration and ρ_s is the density of particle.

3. Results and discussion

The governing equations and the associated boundary conditions are solved numerically by FIDAP, a commercial software based on a finite element scheme. The applicability of the numerical method adopted is justified by comparing the drag force evaluated by the present method when $D\to\infty$, F_D^∞, with the corresponding value of Machač et al. [7], F_D'. In the latter, Eqs.

Table 2
Comparison between the drag force evaluated by the present method when $D\to\infty$, F_D^∞, with the corresponding result of Machač et al. [7], F_D', at various n, (a), and at various λ, (b), for the case when $L/d_c=1.0$

(a)			
$\lambda=0.1887$ s	$n=0.2$	$n=0.5$	$n=0.8$
u_∞ (cm/s)	10.1742	4.1898	3.1972
F_D^∞(g cm/s^2)	65.0442	65.0442	65.0442
F_D' (g cm/s^2)	110.1332	63.0098	59.7932
(b)			
$n=0.5$	$\lambda=0.1887$ s	$\lambda=5.1887$ s	$\lambda=9.1887$ s
u_∞ (cm/s)	1.0086	6.5841	10.0590
F_D^∞ (g cm/s^2)	21.0000	21.0000	21.0000
F_D' (g cm/s^2)	18.1583	22.6390	22.2466

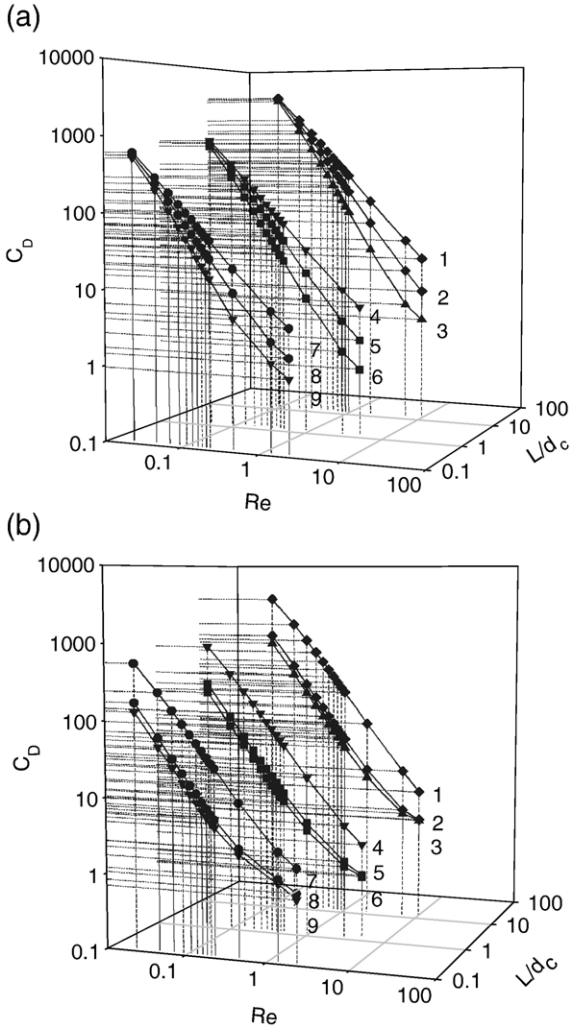

Fig. 2. (a) Variation of drag coefficient C_D as a function of Re and L/d_c at various values of n with $d_c/D=0.1$ and $\lambda=0.1887$ s. Curves 1, 4, and 7, $n=0.8$, curves 2, 5, and 8, $n=0.5$, curves 3, 6 and 9, $n=0.2$. (b) Variation of C_D as a function of Re and L/d_c at various values of λ with $d_c/D=0.1$ and $n=0.5$. Curves 1, 4, and 7, $\lambda=0.1887$ s, curves 2, 5, and 8, $\lambda=5.1887$ s, curves 3, 6, and 9, $\lambda=9.1887$ s.

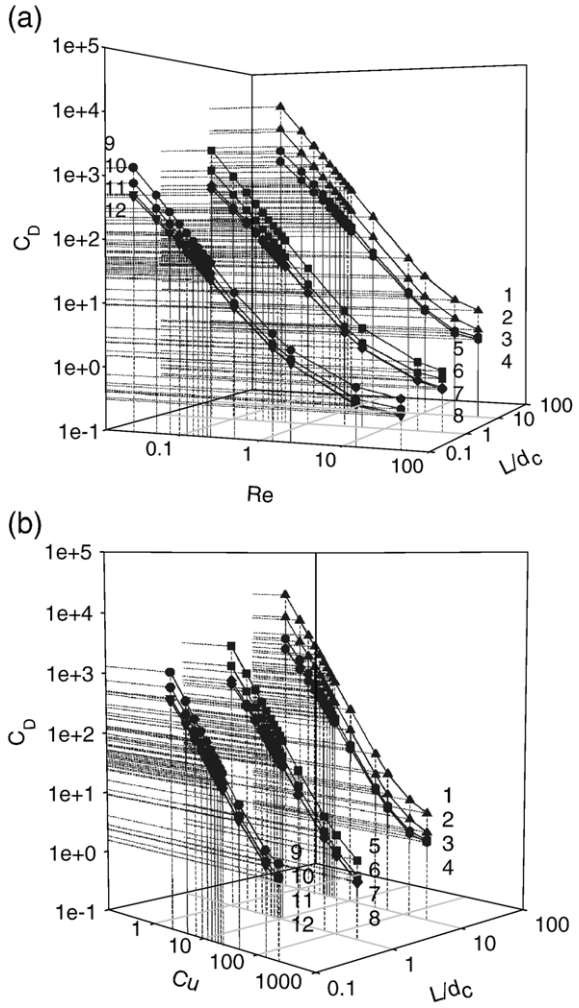

Fig. 3. Variations of drag coefficient C_D as a function of Re and (L/d_c) at various values of (d_c/D) with $n=0.5$ and $\lambda=0.1887$ s, (a), and those as a function of Cu and (L/d_c), (b). Curves 1, 5, and 9, $d_c/D=0.5$, curves 2, 6, and 10, $d_c/D=0.3$, curves 3, 7, and 11, $d_c/D=0.1$, curves 4, 8, and 12, $d_c/D=0.03$.

(12) and (13) are used to obtain Z and φ_N, the results substituted into Eq. (11) to evaluate C_D, and F_D' is calculated by

$$F_D = C_D A_n \left(\frac{\rho u_t^2}{2}\right) \tag{15}$$

where A_n is the projection area of a particle on a plane perpendicular to its movement. The value of F_D^∞ is obtained by extrapolating the terminal velocity of a particle based on the present result to the case when $D\to\infty$ and then using Eqs. (11), (12), (13). The results obtained are summarized in Tables 1–3. Considering the fact that Eqs. (12) and (13) are of empirical nature, the agreement between F_D^∞ and F_D' is satisfactory. The large difference between the two at $n=0.2$ arises from that Eq. (13) is applicable to $0.3<n<1.0$ only. For illustration, the diameter of a particle is fixed in following discussions. Here, we assume that a cylindrical pore is infinitely long, which is checked by examining if the outflow boundary conditions are satisfied at a point far away from particle. Numerical calculation reveals that a point about twenty times of particle radius apart from a particle can be assumed far enough. This criterion is used in all numerical simulations.

The simulated variations of the drag coefficient C_D as a function of Re and (L/d_c) at various values of n are shown in Fig. 2a, and those at various values of λ are illustrated in Fig. 2b. It is known that for Newtonian fluid at low Reynolds number, Stokes law is applicable, that is, $\log(C_D)$ is linearly dependent on $\log(Re)$ with slope −1. Fig. 2 reveals that the more significant the shear-thinning nature of a Carreau fluid, that is, the smaller the value of n or the larger the value of λ, the smaller the value of Re at which a $\log(C_D)$–$\log(Re)$ curve starts to deviate from a Stokes-law like relation. Also, the longer the particle is, the faster the rate of decrease of C_D as Re increases and the larger the value of Re at which the $\log(C_D)$–$\log(Re)$ curve starts to deviate from a Stokes-law like relation. These can be explained by that a smaller value of n or a larger value of λ leads to a faster decrease in the rate of apparent viscosity with the increase in the shear rate. Since a decrease in the apparent viscosity of a fluid is equivalent to an increase in the mean Reynolds number of the corresponding flow field, this leads to a greater excess pressure on the leading surface of a particle. If the fluid surrounding a

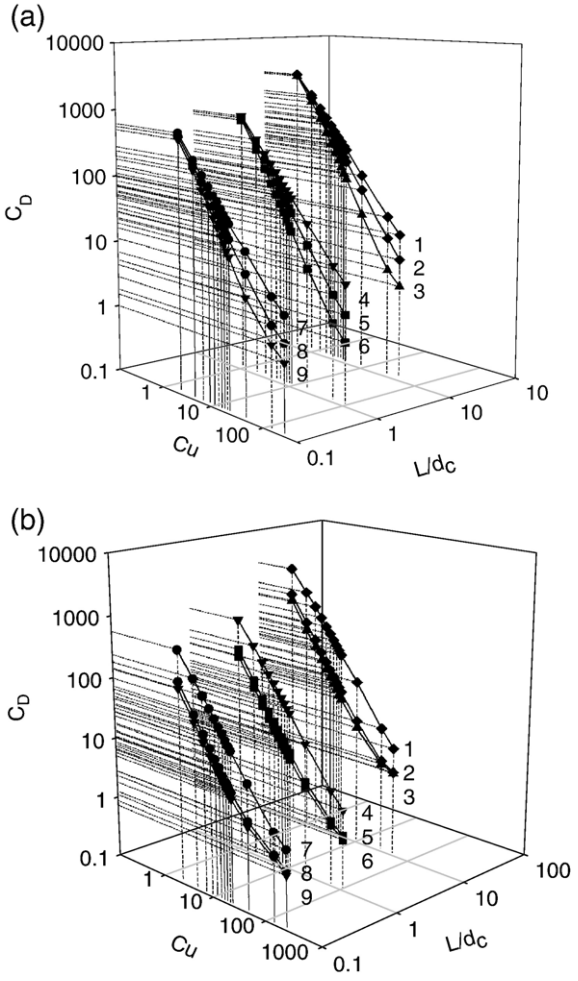

Fig. 4. Variation of drag coefficient C_D as a function of Cu and (L/d_c) with $d_c/D=0.1$. (a) Curves 1, 4, and 7, $n=0.8$, curves 2, 5, and 8, $n=0.5$, curves 3, 6, and 9, $n=0.2$. (b) Curves 1, 4, and 7, $\lambda=0.1887$ s, curves 2, 5, and 8, $\lambda=5.1887$ s, curves 3, 6, and 9, $\lambda=9.1887$ s.

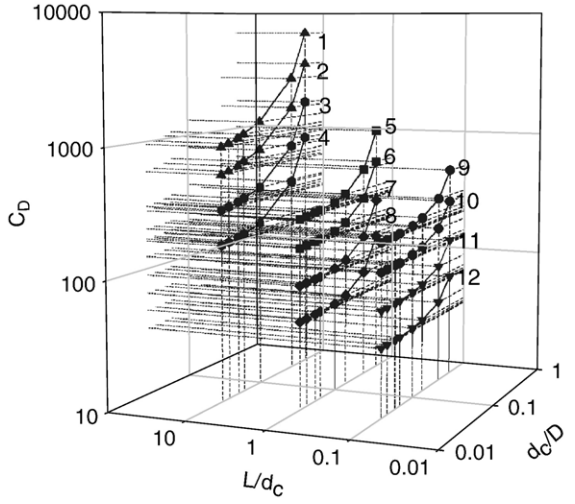

Fig. 5. Variation of drag coefficient C_D as a function of (L/d_c) and (d_c/D) at various values of u_t with $n=0.5$ and $\lambda=0.1887$ s. Curves 1, 5, and 9, $u_t=8$ cm/s, curves 2, 6, and 10, $u_t=5$ cm/s, curves 3, 7, and 11, $u_t=3$ cm/s, curves 4, 8, and 12, $u_t=2$ cm/s.

particle is unable to fill the space arising from its movement in time, the flow field near the leading surface of the particle becomes asymmetric to that near its rear surface, and the log (C_D)–log(Re) curve deviates from the corresponding Stokes-law like relation. If a particle is long, the gap between the particle and the pore is also long, and, therefore, it is easier for the flow field to remain symmetric. This is not the case for a short particle, and its two ends have a greater influence on the nearby flow field than a long particle having the same ends does. Therefore, C_D for a longer particle is larger than that for a shorter particle. For example, if both Re and λ are fixed, C_D at $L/d_c=10$ in Fig. 2b is larger than that at $L/d_c=0.1$.

Fig. 3a suggests that when a particle is sufficiently away from the wall of a tube (d_c/D is small) C_D is insensitive to the variation of particle-wall distance. On the other hand, if it is sufficiently close to the wall, the longer it is the more sensitive the variation of its C_D as particle-wall distance varies. For instance, at $Re=10$ and $L/d_c=10$, C_D increases from 5.5 to 21 as (d_c/D) increases from 0.03 to 0.5, but it increases from 0.8 to 1.6 when $L/d_c=0.1$. However, as will be discussed later, this does not mean that the influence of boundary on the wall factor f for a longer particle is more significant than that for a shorter particle. Fig. 3b shows the variations of C_D as a function of Cu and (L/d_c) at various values of (d_c/D), and those at various values of n and λ are presented in Fig. 4. Since the larger the value of Cu the more important the shear-thinning nature of a Carreau fluid, the behavior of C_D observed in Figs. 3b and 4 can be explained by the same reasoning as those employed in the discussions of Fig. 2.

The influence of the presence of a boundary, measured by (d_c/D), and that of the scaled length of a particle on its drag coefficient at various terminal velocities are illustrated in Fig. 5. This figure reveals that the qualitative behaviors of the variation of C_D as a function of (d_c/D) are the same at various u_t. Quantitatively, the longer the particle, the faster the rate of increase of C_D as (d_c/D) increases.

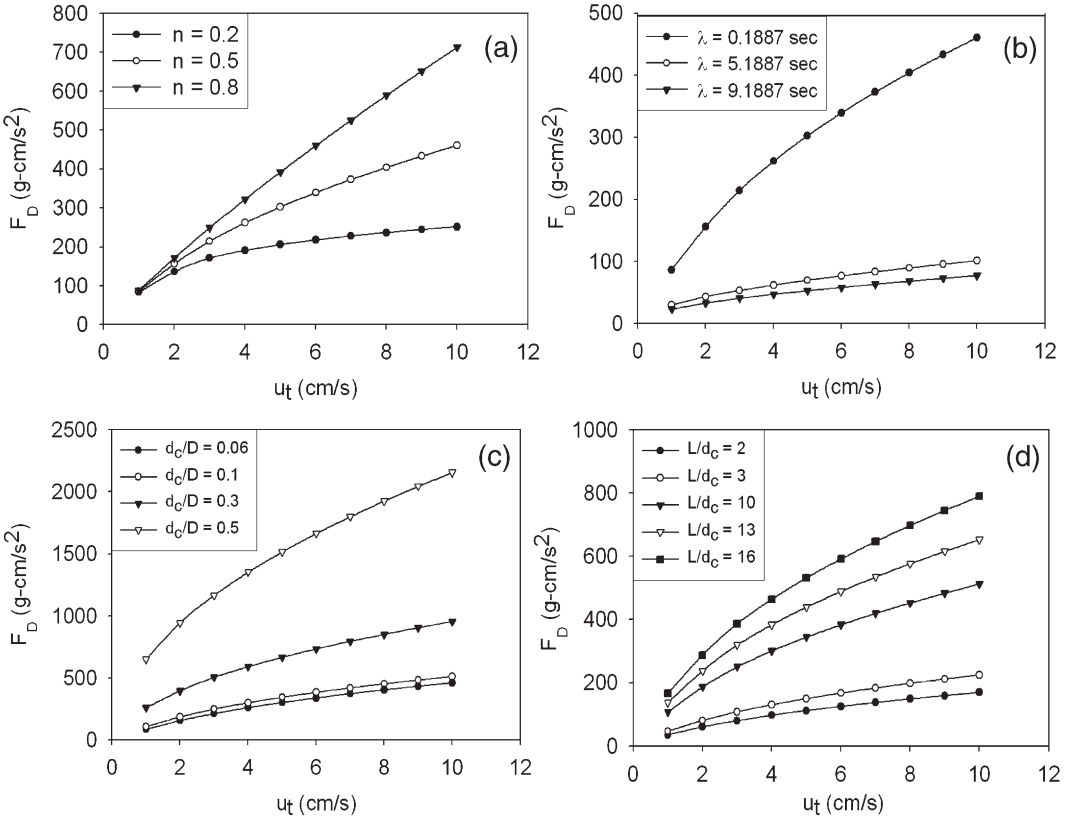

Fig. 6. Variation of drag force F_D as a function of u_t. (a) $L/d_c=10.0$, $d_c/D=0.1$, $\lambda=0.1887$ s, n varies; (b) $L/d_c=10.0$, $d_c/D=0.1$, $n=0.5$, λ varies; (c) $n=0.5$, $\lambda=0.1887$ s, $L/d_c=10.0$, d_c/D varies; (d) $n=0.5$, $\lambda=0.1887$ s, $d_c/D=0.1$, L/d_c varies.

Fig. 6 shows the drag on a particle as a function of its terminal velocity at various values of n, λ, (d_c/D), and (L/d_c). Fig. 6a and b indicate that for a fixed u_t, the smaller the value of n or the larger the value of λ the smaller the value of F_D is. This is expected since the shear-thinning nature of a Carreau fluid is significant under these conditions. Fig. 6a and b also suggest that

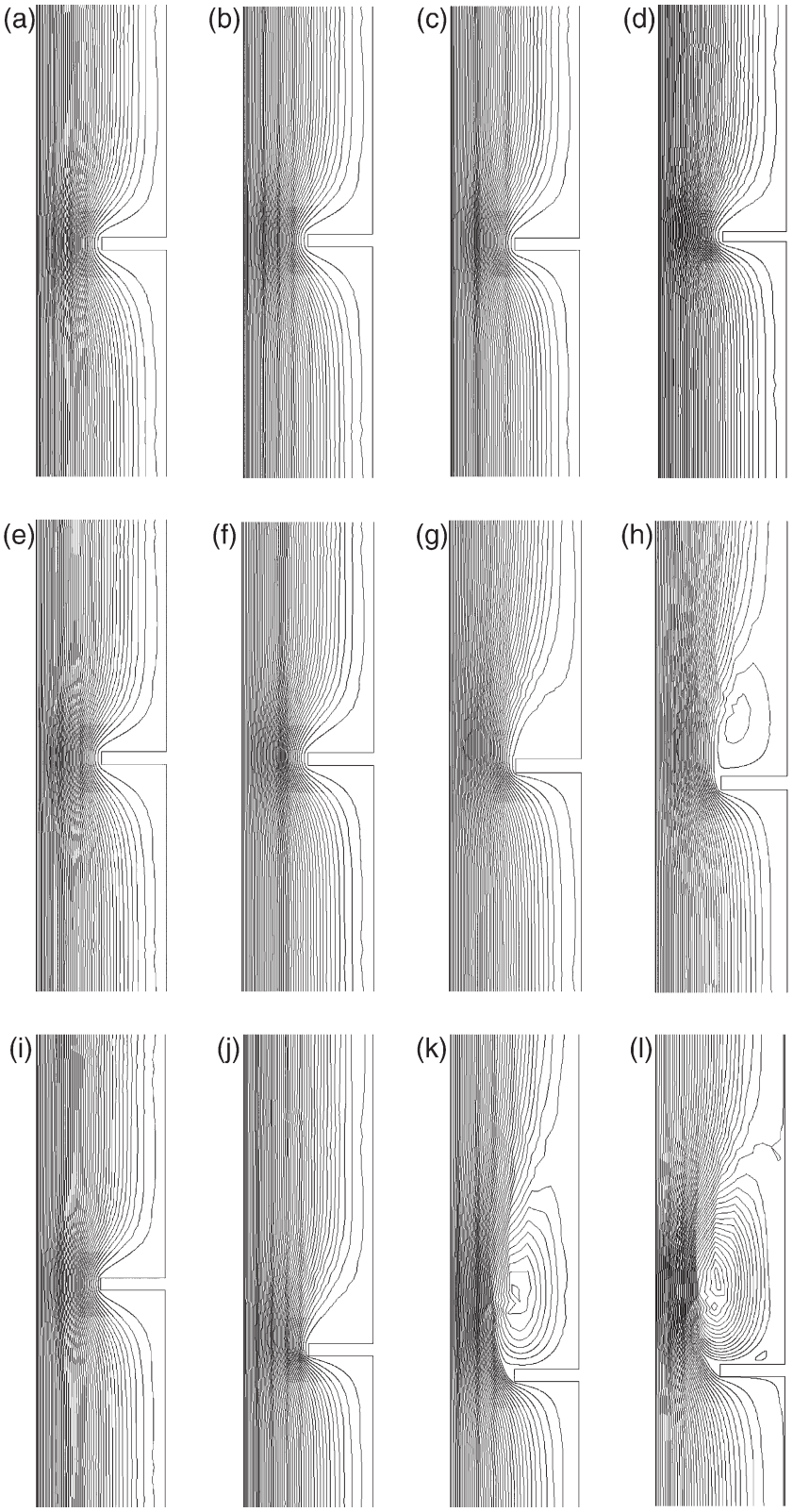

Fig. 7. Contours of streamline with $L/d_c=0.1$, $d_c/D=0.5$, and $\lambda=0.1887$ s. (a)–(d), $n=0.8$, (e)–(h), $n=0.5$, (i)–(l), $n=0.2$. (a), (e), and (i), $u_t=5.0$ cm/s, (b), (f), and (j), $u_t=20.0$ cm/s, (c), (g), and (k), $u_t=60.0$ cm/s, (d), (h), and (l), $u_t=100.0$ cm/s.

the smaller the value of n or the larger the value of λ the slower the rate of increase of F_D as u_t increases. According to Fig. 6c and d, if u_t is fixed, the larger the value of (d_c/D) (boundary effect is more significant) or the larger the value of (L/d_c) (longer particle) the larger the value F_D and the faster the rate of increase of F_D as u_t increases.

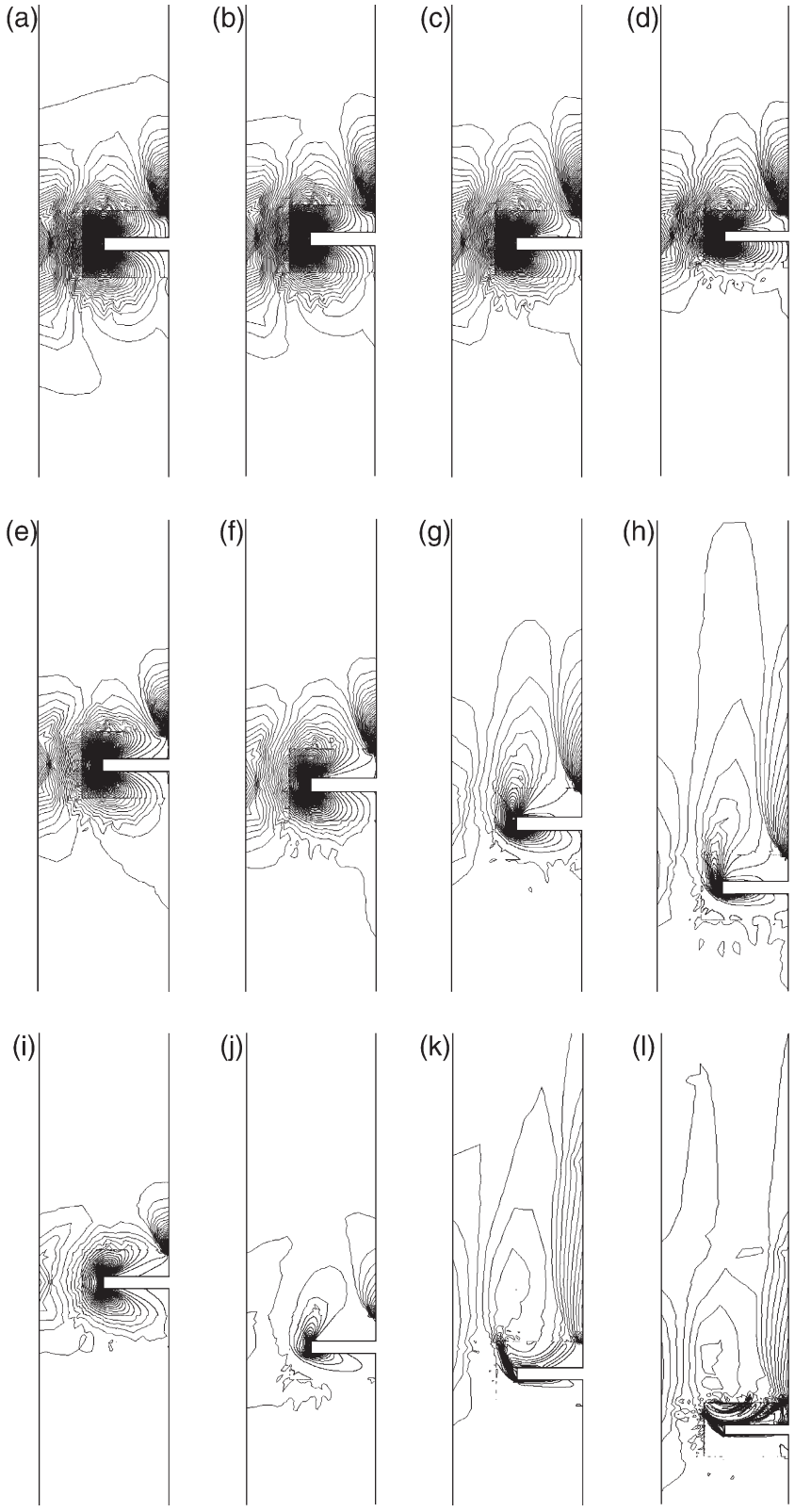

Fig. 8. Contours of vorticity with $L/d_c=0.1$, $d_c/D=0.5$, and $\lambda=0.1887$ s. (a)–(d), $n=0.8$, (e)–(h), $n=0.5$, (i)–(l), $n=0.2$. (a), (e), and (i), $u_t=5.0$ cm/s, (b), (f), and (j), $u_t=20.0$ cm/s, (c), (g), and (k), $u_t=60.0$ cm/s, (d), (h), and (l), $u_t=100.0$ cm/s.

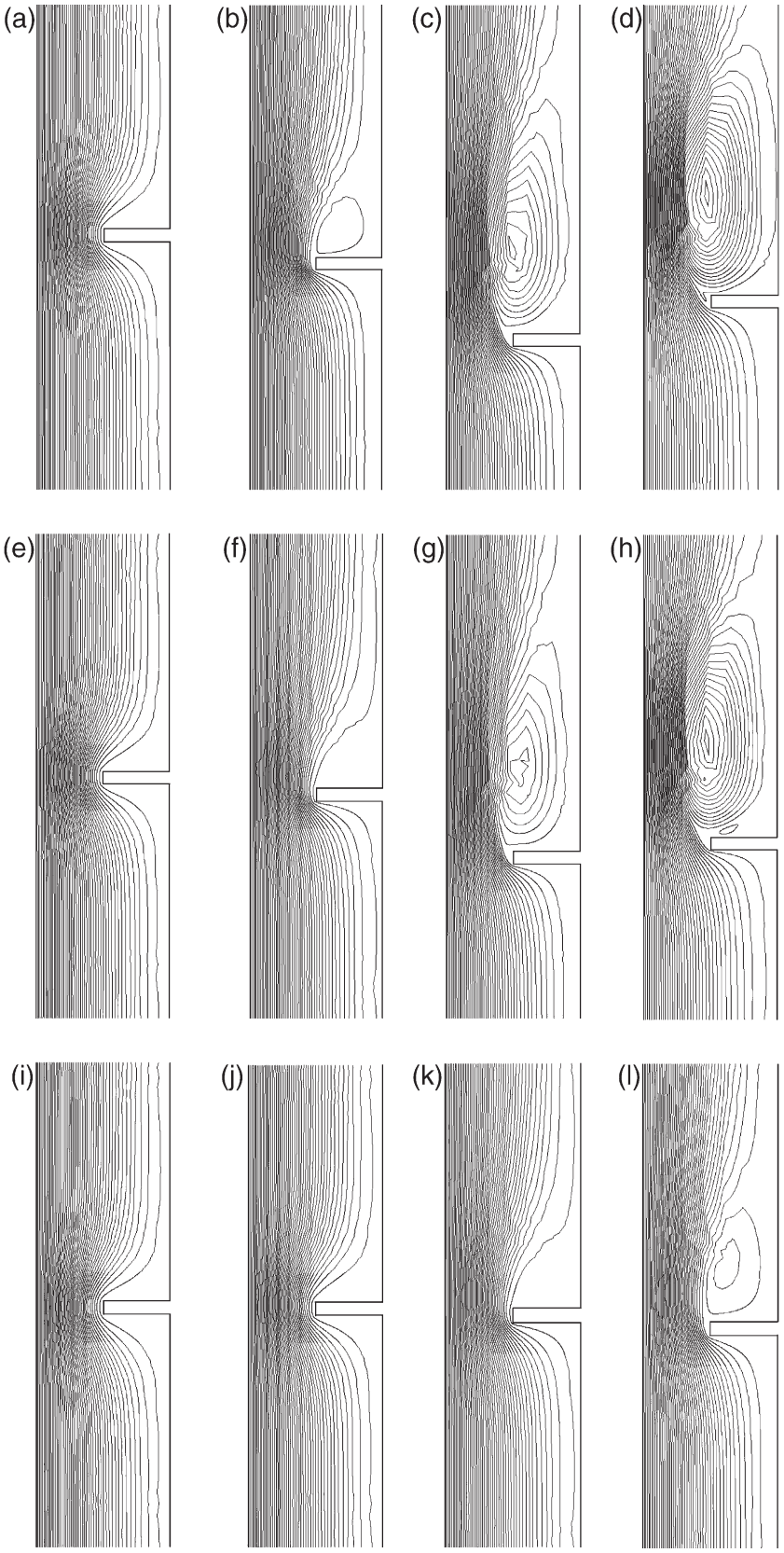

Fig. 9. Contours of streamline with $L/d_c=0.1$, $d_c/D=0.5$, and $n=0.5$. (a)–(d), $\lambda=9.1887$s, (e)–(h), $\lambda=5.1887$s, (i)–(l), $\lambda=0.1887$ s. (a), (e), and (i), $u_t=5.0$ cm/s, (b), (f), and (j), $u_t=20.0$ cm/s, (c), (g), and (k), $u_t=60.0$ cm/s, (d), (h), and (l), $u_t=100.0$ cm/s.

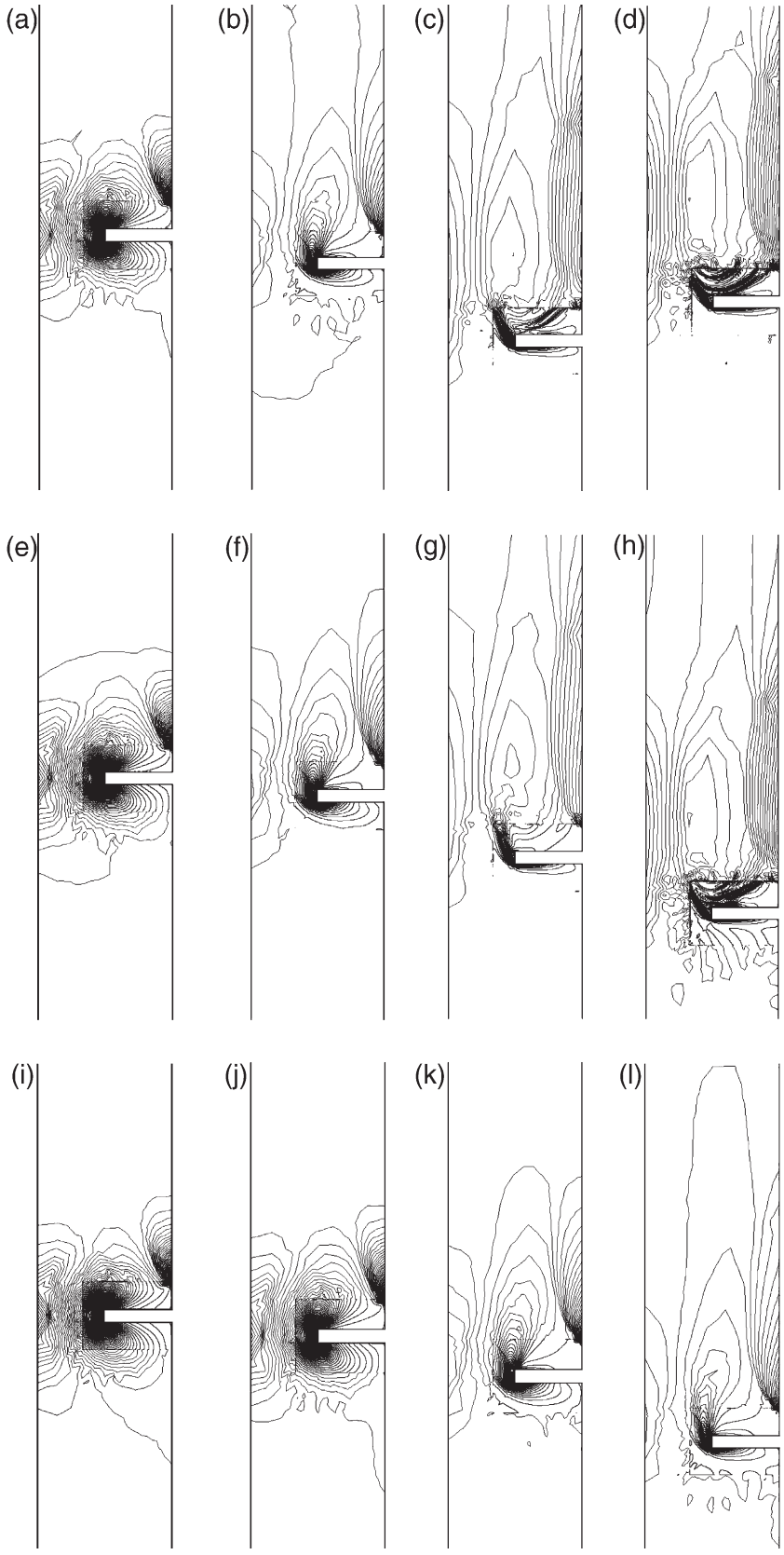

Fig. 10. Contours of vorticity with $L/d_c=0.1$, $d_c/D=0.5$, and $n=0.5$. (a)–(d), $\lambda=9.1887$ s, (e)–(h), $\lambda=5.1887$ s, (i)–(l), $\lambda=0.1887$ s. (a), (e), and (i), $u_t=5.0$ cm/s, (b), (f), and (j), $u_t=20.0$ cm/s, (c), (g), and (k), $u_t=60.0$ cm/s, (d), (h), and (l), $u_t=100.0$ cm/s.

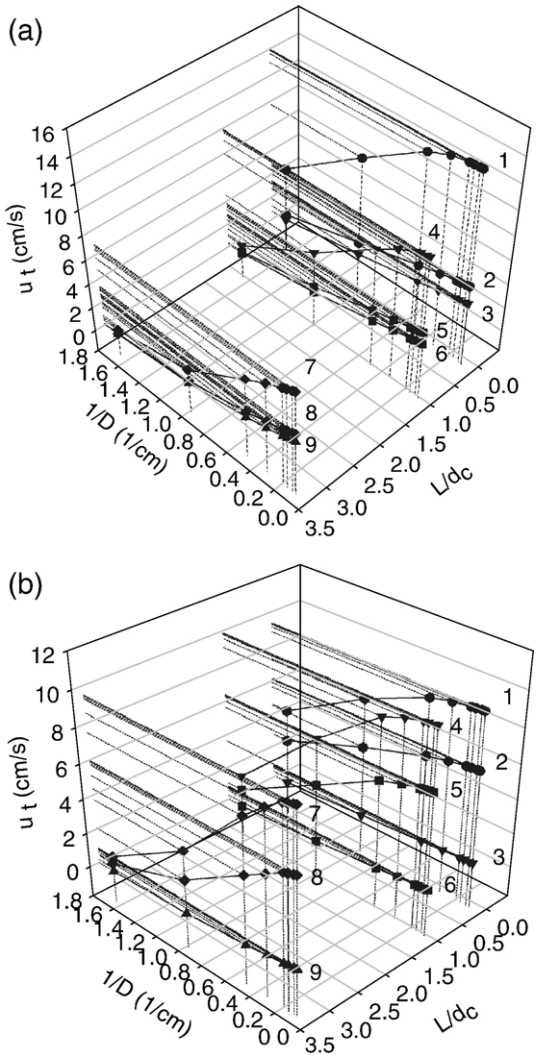

Fig. 11. (a) Variation of u_t as a function of $(1/D)$ at various values of n with $\lambda=0.1887$ s. Curves 1, 4, and 7, $n=0.2$, curves 2, 5, and 8, $n=0.5$, curves 3, 6, and 9, $n=0.8$. (b) Variation of u_t as a function of $(1/D)$ at various values of λ with $n=0.5$. Curves 1, 4, and 7, $\lambda=9.1887$ s, curves 2, 5, and 8, $\lambda=5.1887$ s, curves 3, 6, and 9, $\lambda=0.1887$ s.

If the velocity of a particle is slow, the flow field near its leading surface is symmetric to that near its rear surface, as can be seen in Figs. 7 and 8. However, if its velocity is sufficiently fast, wakes are formed near its rear surface and the flow fields become asymmetric, which explains why a $\log(C_D)$–$\log(Re)$ curve deviates from the corresponding Stokes-law like relation. Since the smaller the value of n the more asymmetric the flow fields, Figs. 7 and 8 imply that the smaller the value of n the smaller the value of C_D, which is observed in Fig. 2a. Similarly, the observation that the larger the value of λ the smaller the value of C_D shown in Fig. 2b can be explained by the behaviors of the flow field shown in Figs. 9 and 10.

At steady state, the sum of the drag force, F_D, and the buoyant force, F_B, is balanced by the gravitational force, F_G. For a given particle in a fluid of fixed density, since both F_B and F_G are fixed, so is F_D. That is, F_D is uninfluenced either by the presence of a boundary or by the terminal velocity of the particle. This nature can be used to obtain the variation of the terminal velocity of a particle as a function of the significance of boundary effect. In Fig. 6c, for example, if F_D is fixed, u_t at different (d_c/D) can be determined, and if d_c is given, a u_t against $(1/D)$ curve such as that presented in Fig. 11 can be constructed. Note that an extrapolating of the curve in this figure to $1/D=0$ yields the terminal velocity when a boundary is absent, u_∞. The influence of a boundary on the terminal velocity of a particle can be measured by the wall factor f defined by $f=u_t/u_\infty$. Apparently, the closer the value of f to unity the less significant the boundary effect is. According to Chhabra [5], for a disk in a cylinder filled with a shear-thinning, power-law fluid, f (or u_t) is proportional to $(1/D)$ if $Re<7$ and $d_v/D<0.5$. Fig. 11a shows that this relation

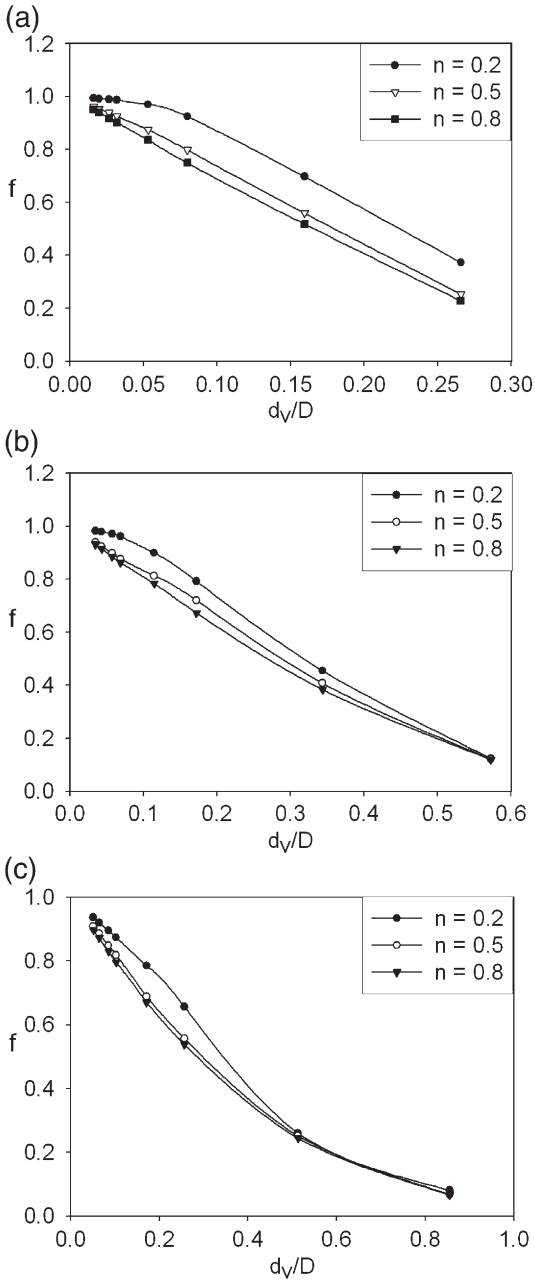

Fig. 12. Variation of f as a function of (d_v/D) at various values of n with $\lambda=0.1887$ s. (a) $L/d_c=0.1$ and $F_D=55.4193$ g cm/s^2, (b) $L/d_c=1.0$ and $F_D=65.0443$ g cm/s^2, (c) $L/d_c=3.33$ and $F_D=100.0503$ g cm/s^2.

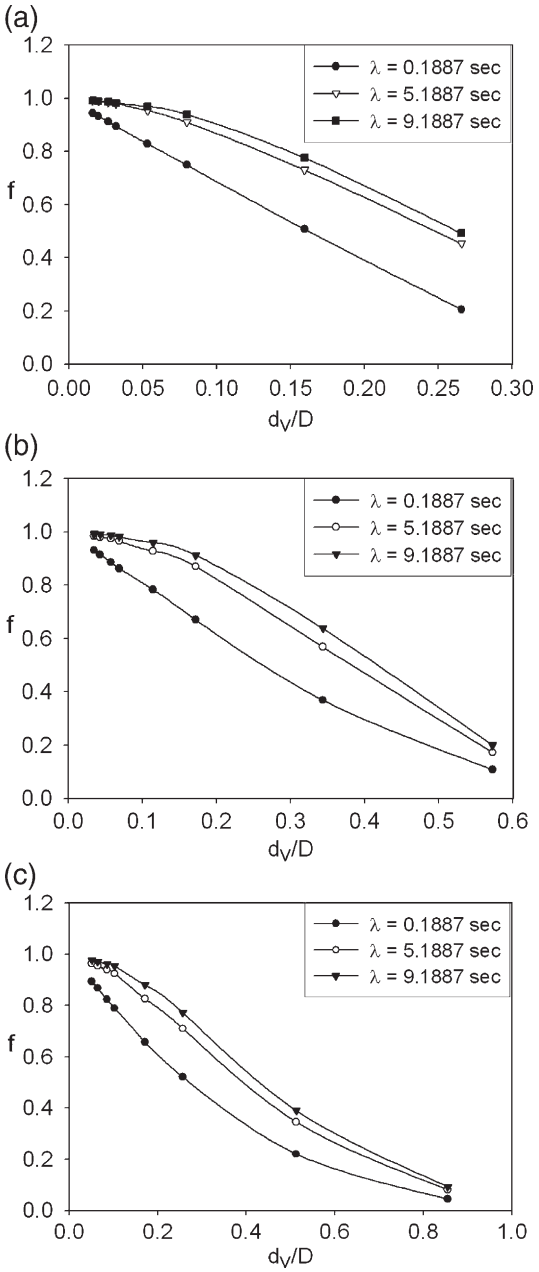

Fig. 13. Variation of f as a function of (d_v/D) at various values of λ with $n=0.5$. (a) $L/d_c=0.1$ and $F_D=14.6874$ g cm/s^2, (b) $L/d_c=1.0$ and $F_D=21.0$ g cm/s^2, (c) $L/d_c=3.33$ and $F_D=34.0$ g cm/s^2.

is applicable for $(1/D)$ sufficiently large, that is, a particle is sufficiently close to a boundary, but if a particle is away from the boundary, then that relation becomes nonlinear. Fig. 11 reveals that the more significant the shear-thinning nature of a Carreau fluid the faster the terminal velocity and the faster is its rate of decrease as a boundary is approached. Also, the closer a Carreau fluid to a Newtonian fluid the closer a u_t against $(1/D)$ curve to a straight line. Figs. 12 and 13 indicate that for a fixed value of (d_v/D), the value of f for a longer particle is closer to unity than that of a shorter particle, that is, the former is less influenced by the boundary. As pointed out previously, for a given particle in a fluid of fixed density, the drag acting on it is fixed. Therefore, if u_t is smaller, which occurs when $(1/D)$ increases (particle is close to boundary) or when the shear-thinning nature of a fluid is less significant, the contribution to the drag by shear stress is more important. On the other hand, if u_t is larger, the contribution to the drag by normal stress is more important. Because the main retardation force comes from the normal stress in sedimentation, the rate of decrease in the terminal velocity is faster when a particle is far away from boundary. On the other hand, the decrease of that rate becomes slower when a boundary is approached. In Fig. 11a with $n=0.2$, for example, if $1/D<1.0$, u_t is large, the corresponding normal stress is large, and the rate of decrease of u_t is also large; if $1/D>1.0$, u_t is small, so is its rate of decrease. The above discussions imply that a u_t against $(1/D)$ curve can have an inflection point. Fig. 11 indicates that the smaller the value of n or the larger the value of λ, that is, the more significant the shear-thinning nature of a Carreau fluid, the more appreciable the presence of the inflection point. Also, the longer the particle the smaller the value of $(1/D)$ at which the inflection point occurs. Note that this inflection point is not observed for the case of a Newtonian fluid at a low to medium value of Re.

Fig. 14 shows the variation of the terminal velocity of a particle as a function of $(1/D)$ and that of the wall factor as a function of (d_v/D) for four different particles, each has the same shape but with different weights. Note that in this case, the heavier a particle is the greater the drag force acting on it. Fig. 14a shows that the heavier a particle is the faster the rate of decrease in its terminal velocity as $(1/D)$ increases (the size of boundary

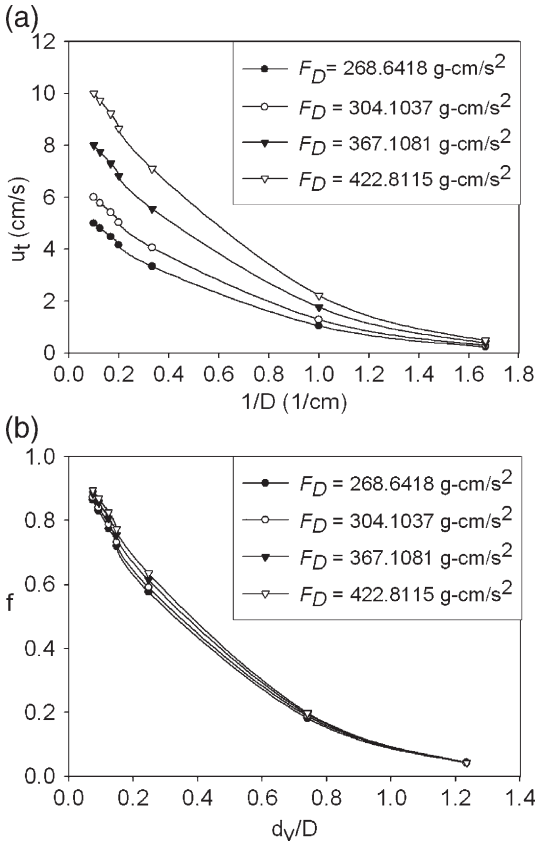

Fig. 14. (a) Variation of u_t as a function of $(1/D)$ at various values of F_D. (b) Variation of f as a function of (d_v/D) at various values of F_D. Parameters used are $L/d_c=10.0$, $n=0.5$, and $\lambda=0.1887$ s.

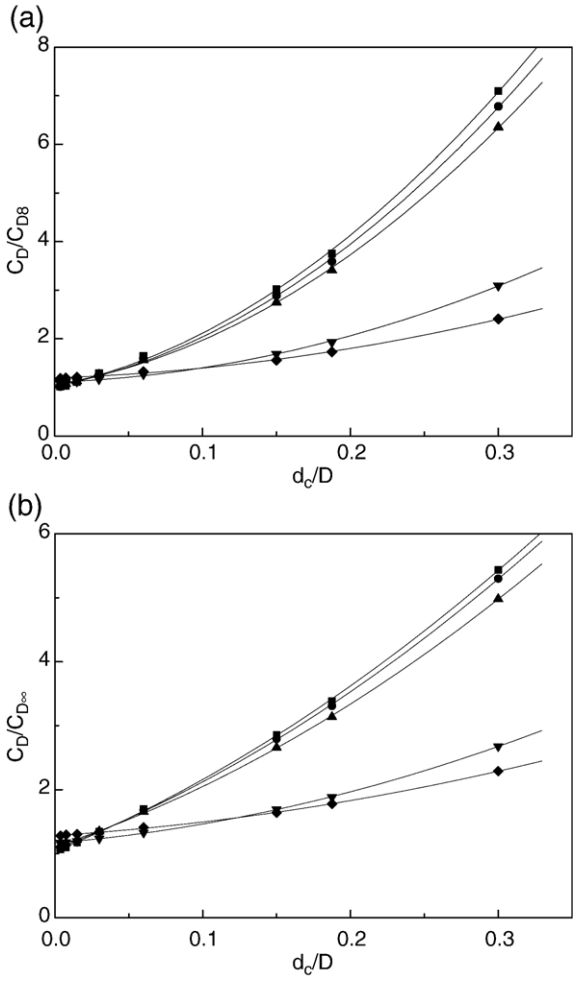

Fig. 15. Variation of $(C_D/C_{D\infty})$ as a function of (d_c/D) for various values of L/d at two levels of u_t for the case when $n=0.5$ and $\lambda=0.1887$. Solid curves represent the fitted polynomial relationship described by Eq. (16) with values of adjustable parameters summarized in Table 4. (a) $u_t=0.2$, (b) $u_t=1.0$. ■ $L/d_c=16.67$; ● $L/d_c=13.33$; ▲ $L/d_c=10.0$; ▼ $L/d_c=1.0$; ●● $L/d_c=0.1$.

decreases). The terminal velocities of the four particles are close to each other if $(1/D)$ is sufficiently large. According to Fig. 14b, the f of a heavier particle is larger than that of a lighter particle. This implies that the influence of boundary on the terminal velocity of a heavier particle is less significant than that of a lighter particle.

Let $C_{D\infty}$ be the drag coefficient evaluated by Eq. (11), which is used by Machač [7] for the unconfined case at a low Reynolds number and C_D be the corresponding drag coefficient in the present case where a cylindrical boundary is present. Fig. 15 shows the variation of (C_D/C_{D_∞}) as a function of (d_c/D) at two levels of u_t. This figure suggests that the following empirical relation is appropriate:

$$\left(\frac{C_D}{C_{D_\infty}}\right) = A + B_1\left(\frac{d_c}{D}\right) + B_2\left(\frac{d_c}{D}\right)^2 \qquad (16)$$

The fitted values of the adjustable parameters A, B_1, and $B2$ are summarized in Table 4. This table indicates that the values of the adjustable parameters are influenced by u_t.

4. Conclusions

In summary, the drag on a cylindrical particle moving along the axis of a cylindrical tube filled with a Carreau fluid is analyzed, and the influences of the key parameters of the system under consideration, including the relaxation time constant and the power-law index of the fluid, the length of a particle, and the diameter of a cylindrical tube, on the drag coefficient and the associated flow field are discussed. The results of numerical simulation yield the following observations: (a) The more significant the shear-thinning nature of a Carreau fluid the smaller the value of the Reynolds number at which a log(drag coefficient)–log(Reynolds number) curve starts to deviate from a linear relation. Also, the longer the particle is, the faster the rate of decrease of drag coefficient as Reynolds number increases and the larger the value of Reynolds number at which the log(drag coefficient)–log(Reynolds number) curve starts to deviate from a linear relation. (b) If a particle is sufficiently away from the wall of a tube, the drag coefficient is insensitive to the variation of particle-wall distance. On the other hand, if it is sufficiently close to the wall, the longer it is the more sensitive the variation of its drag coefficient as particle-wall distance varies. (c) For a given particle and fluid, while the terminal velocity of the former is influenced by the presence of a boundary, the drag on the former when it reaches the terminal velocity is uninfluenced either by the presence of a boundary or by its terminal velocity. (d) If a particle is sufficiently close to the wall of a tube, the wall factor is linearly dependent on (1/tube diameter), but if it is away from the wall, they are non-linearly correlated. (e) The more significant the shear-thinning nature of a Carreau fluid the faster the terminal velocity and the faster is its rate of decrease as a boundary is approached. Also, the closer a Carreau fluid to a Newtonian fluid the closer a terminal velocity against (1/tube diameter) curve to a straight line. (f) The terminal velocity of a longer particle is less influenced by a boundary than that of a shorter particle. (g) A terminal velocity against (1/tube diameter) curve can have an inflection point, and the more significant the shear-thinning nature of a Carreau fluid the more appreciable the presence of the inflection point. Also, the longer the particle the smaller the value of (1/tube diameter) at which the inflection point occurs. The inflection point is not observed for the case of a Newtonian fluid at a low to medium value of Reynolds number. (h) For a fixed geometry, the influence of boundary on the terminal velocity of a heavier particle is less significant than that of a lighter particle.

Table 4
Values of the adjustable parameters of the empirical relation, Eq. (16), for the data shown in Fig. 15

	A		B_1		B_2	
L/d	$u_t=0.1$	$u_t=1.0$	$u_t=0.1$	$u_t=1.0$	$u_t=0.1$	$u_t=1.0$
0.1	1.1933	1.2834	1.0506	1.4983	9.9172	6.1702
1	1.1056	1.1660	1.1371	1.9414	18.2072	10.3044
10	1.0553	1.1100	4.8948	7.6423	42.3449	17.4899
13.33	1.0282	1.0693	5.5627	8.7542	45.1227	17.7455
16.67	1.0201	1.0364	6.2881	9.5059	46.2833	17.0942

Acknowledgment

This work is supported by the National Science Council of the Republic of China.

References

[1] A. Tripathi, R.P. Chhabra, T. Sundararajan, Int. Eng. Chem. Res. 33 (1994) 403.
[2] A. Tripathi, R.P. Chhabra, AIChE J. 41 (1995) 728.
[3] K.A. Missirlis, D. Assimacopoulos, E. Mitsoulis, R.P. Chhabra, J. Non-Newton. Fluid Mech. 96 (2001) 459.
[4] R.P. Chhabra, S. Agarwal, K. Chaudhary, Powder Technol. 129 (2003) 53.
[5] R.P. Chhabra, Powder Technol. 88 (1996) 39.
[6] I. Machač, B. Šiška, L. Machačcvá, Chem. Eng. Proc. 39 (2000) 365.
[7] I. Machač, B. Šiška, R. Teichman, Chem. Eng. Proc. 41 (2002) 577.
[8] R.P. Chhabra, P.H.T. Uhlherr, Can. J. Chem. Eng. 58 (1980) 124.
[9] J. Blackery, E. Mitsoulis, J. Non-Newton. Fluid Mech. 70 (1997) 59.
[10] A. Unnikrishnan, R.P. Chhabra, Can. J. Chem. Eng. 69 (1991) 729.
[11] R.P. Chhabra, Can. J. Chem. Eng. 70 (1992) 385.
[12] J.P. Hsu, Y.H. Hsieh, S. Tseng, J. Colloid Interface Sci. 284 (2005) 729.
[13] R.B. Bird, R.C. Armstrong, O. Hassager, Dynamics of Polymer Liquids, vol. 1, Wiley, New York, 1987.
[14] J.P. Hsu, C.F. Shie, S. Tseng, J. Colloid Interface Sci. 286 (2005) 392.